






Original Article


Damage characteristics and new constitutive model of sandstone under wet–dry cycles

HUANG Zhen^{1,2}  <https://orcid.org/0000-0003-2026-5893>; e-mail: hzcslg@163.com

ZHANG Wei¹  <https://orcid.org/0000-0002-1152-1130>; e-mail: zw971126la_lune@163.com

ZHANG Hai¹  <https://orcid.org/0000-0003-2235-7687>;  e-mail: zhanghai19960510@163.com

ZHANG Jia-bing^{1,2}  <https://orcid.org/0000-0002-3421-4926>; e-mail: zhang_jb1@sohu.com

HU Zhao-jian¹  <https://orcid.org/0000-0003-2649-3897>; e-mail: hhhuzj@163.com

*Corresponding author

¹ School of Civil Engineering and Architecture, Guangxi University, Nanning 530004, China

² Key Laboratory of Engineering Disaster Prevention and Structural Safety, Guangxi University, Nanning 530004, China

Citation: Huang Z, Zhang W, Zhang H, et al. (2022) Damage characteristics and new constitutive model of sandstone under wet–dry cycles. *Journal of Mountain Science* 19(7). <https://doi.org/10.1007/s11629-021-7239-8>

© Science Press, Institute of Mountain Hazards and Environment, CAS and Springer-Verlag GmbH Germany, part of Springer Nature 2022

Abstract: The mechanical properties of rock deteriorate under repeated wet-dry (WD) cycles, causing the deformation and failure of the rock mass. A reasonable damage constitutive model can truly reflect the whole process of rock deformation and failure. Therefore, it is of great significance to study the damage characteristics and constitutive behaviour of rock subjected to numerous WD cycles. First, sandstone from Tingliang tunnel was sampled for the WD cycle experiment, and uniaxial and triaxial tests were carried out on the rock samples after various numbers of WD cycles to analyze their macroscale damage characteristics. Then, the damage mechanisms of the rock samples under the action of WD cycling were identified by X-ray diffraction (XRD) and scanning electron microscopy (SEM). Finally, based on the test data, the WD cycle-induced damage variable, Weibull distribution function, damage threshold, Drucker-Prager (D-P) yield criterion and residual strength correction coefficient were introduced, a wet–dry loading (WDL) constitutive damage model that considers the cracking stress of rock masses was established, and the expressions of

the corresponding parameters were given. The results show that an increasing number of WD cycles induces considerable variations in the macroscopic physical and mechanical parameters (such as the rock sample mass, saturated water content, longitudinal-wave velocity, compressive strength and elastic modulus), and the rate of change presents two stages, the inflection point of their rate of change is the 15th WD cycle. Microscopically, the rock sample structure changes from intact and dense to fragmented and unconsolidated; additionally, the surface roughness increases, and the mineral composition changes. The established constitutive damage model exhibited good agreement with the experimental data; thus, this model can reflect the deformation and failure of rocks under WDL conditions, and the physical meaning of each parameter is clear.

Keywords: Wet–dry cycle; Sandstone; Rock damage; Constitutive model

1 Introduction

Ever since Obyhhkob proposed the term “water–

Received: 21-Nov-2021

Revised: 23-Feb-2022

Accepted: 11-May-2022

rock interaction” in the 1950s (Shen et al. 1993; Shen and Wang 2002), this topic has been a major focus of research in the field of geotechnical engineering (Chen et al. 2019; Ni et al. 2008; Xu et al. 2020). Wet-dry (WD) cycles represent the most common water–rock interactions in nature because most natural rock masses at the surface are fractured, porous materials that are highly vulnerable to water erosion. For instance, the water level of the Three Gorges Reservoir fluctuates cyclically between 145 and 175 m every year, resulting in a 30 m drawdown zone along the sloped reservoir bank (Zhang et al. 2014; Liu et al. 2018; Wang et al. 2020; Fang et al. 2019). Other examples include the periodic WD cycles of open pit slopes and the surrounding rock of tunnels under the alternating action of rainfall and sunshine (Qin et al. 2018; Zeng et al. 2019); the weathering of important cultural relics such as rock paintings, grottoes and historical sites (Lee et al. 2011; Wang et al. 2014; Zhang et al. 2021); and the tidal fluctuations experienced by coastal embankments (Trenhaile 2014). Such WD cycles cause considerable damage to rock masses, the physical and mechanical properties of which are consequently degraded to varying degrees, which has important impacts on geotechnical engineering construction. Therefore, studying the damage mechanisms of rocks under WD cycles and developing constitutive damage models for rocks subjected to wet-dry loading (WDL) are crucial to understanding the deformation and failure processes of different rock masses and have important guiding significance for both theoretical and practical aspects of geotechnical engineering.

In recent years, many scholars have studied the influences of WD cycles on rocks and have reported a variety of successes. For example, Özbek (2013) conducted 50 WD cycle tests on igneous rocks in Central Anatolia and found that their weight, porosity, water absorption, longitudinal-wave velocity and uniaxial compressive strength changed to varying degrees. Gholamreza et al. (2015) conducted WD cycle tests on sandstones from the Upper Red Formation southwest of Qom, Central Iran, and noted that the longitudinal-wave velocity and uniaxial compressive strength decreased after 40 cycles, while Poisson’s ratio gradually increased. Zhao et al. (2018) performed WD cycle tests on Simianshan mudstone samples obtained from southwestern Chongqing, China; the porosity increased significantly after 12 cycles, while the uniaxial compressive strength and elastic modulus

decreased. An et al. (2020) conducted a WD cycle experiment on weathered feldspathic sandstone with distilled water and a saturated Na_2SO_4 solution and reported that the physical and mechanical parameters of the sandstone deteriorated more significantly in the salt solution than in water, with the former resulting in more microcracks and voids. Yuan et al. (2018) conducted WD cycle tests on sandstone in acidic, neutral and alkaline environments (pH=4, 7 and 9, respectively) and considered that the mechanical parameters of the sandstone deteriorated the most in the acidic environment; in addition, the effects of the WD cycles on the mechanical parameters such as the compressive strength, cohesion and internal friction angle were weakened with an increasing number of WD cycles. Liu et al. (2016) performed nondestructive computed tomography (CT) scans and splitting tests on sandstone after being subjected to WD cycles and found that the average CT number and tensile strength on sandstone cross sections decreased with an increasing number of WD cycles. Meng et al. (2020) used acoustic emission equipment to study the relationships between the mechanical parameters of sandstone and the total number of acoustic emissions under the action of WD cycling and proposed that the propagation of microcracks was the main reason for the attenuation of both the mechanical parameters of sandstone and the total number of acoustic emissions. Chen et al. (2018) and Xie et al. (2018) employed scanning electron microscopy (SEM) to investigate granite and sandstone samples, respectively, after numerous WD cycles. Their test results showed that with an increase in the number of WD cycles, rock fragments fell off, microcracks and micropores developed and connected, the sample surfaces changed from smooth to rough, and their structure changed from intact and dense to fractured and unconsolidated.

In terms of theoretical analysis, many scholars have developed constitutive damage models for various rocks. For example, Li et al. (2012), Wang et al. (2007) and Shen et al. (1984) proposed a statistical constitutive model of rock damage due to strain softening based on the basic theory of damage mechanics, the Lemaitre strain equivalence hypothesis (Lemaitre et al. 1984), and the Weibull distribution (Weibull et al. 1951). Wang et al. (2017) proposed an improved Duncan–Chang constitutive model to describe the stress–strain curve of sandstone after WD cycles and verified the model by a numerical simulation in FLAC^{3D}. Du et al. (2019)

asserted that the damage incurred by red sandstone under WD cycles and impact loads could be divided into macrodamage and microdamage and established a coupled constitutive damage model based on the Lemaitre strain equivalence hypothesis; ultimately, the effectiveness of the model was verified by a dynamic compression test on red sandstone. Hu et al. (2018) established a constitutive damage equation under the coupling of WD cycles and loads based on the energy principle and verified the effectiveness of the model by performing a comparison of their findings with those in the literature. Wang et al. (2020) studied a dangerous rock mass in Jianchuan east of the Three Gorges Reservoir area and established a constitutive damage model of the basement rock mass under WD conditions based on indoor test data.

In summary, research on the characteristics of rock subjected to WD cycles has focused mainly on their changes in macrophysical and mechanical properties and microstructure, whereas few studies have discussed the relationships between these features. In addition, the literature on the loading-induced deformation and failure processes of rock after experiencing WD cycles is not complete, and the existing constitutive damage models for rocks under WDL were derived based on the Weibull distribution, but the influences of WD cycles on the distribution parameters were neglected in the derivation. Therefore, this paper analyses and discusses the relationships of the macrophysical and mechanical properties and microstructure of rock by performing sample mass, longitudinal-wave velocity, SEM, X-ray diffraction (XRD) and uniaxial and triaxial tests on sandstone samples after WD cycling. Based on an existing rock constitutive damage model, a WDL constitutive damage model that considers the strength of microelements and satisfies the Drucker-Prager (D-P) yield criterion considering the effects of WD cycles is established by introducing a WD cycle-induced damage variable and a Weibull distribution function. Finally, the rationality and applicability of this model are verified by experimental data.

2 Test

2.1 Test sample preparation

The test samples were selected from Tingliang

tunnel in the city of Chongzuo, Guangxi Zhuang Autonomous Region, China. The formation lithology is grayish yellow siltstone of the second group of Jurassic nadang group (J2nlb). After the rock was obtained in situ, it was sealed, packaged, and sent back to the laboratory for sample processing and preparation. According to the requirements of the Standard for Tests Method of Engineering Rock Masses (GB/T 50266-2013), a cylindrical sample with a diameter of 50 mm and a height of 100 mm was prepared after cutting the mass, drilling a core, and grinding the rock; the upper and lower end faces were ensured to be parallel within ≤ 0.05 mm, and the flatness of the end face was ≤ 0.02 mm. To ensure the accuracy, effectiveness and scientificity of the test and reduce the dispersion of the rock data from the standard, all the rock samples were prepared from the same rock, and nondestructive ultrasonic testing was carried out on the rock samples (Vilhelm et al. 2013; Mckenzie et al. 1982; Fener et al. 2011). Rock samples with similar longitudinal-wave velocities were selected for testing, with a total of 39 test samples being prepared. Then, the physical parameters of the test samples were determined, and the average values among all the samples were taken as the basic physical parameters: the natural density was 2.55 g/cm³, the dry density was 2.53 g/cm³, the water content was 0.71%, and the longitudinal-wave velocity was 3369 m/s.

2.2 Test procedure

According to the requirements of the Standard for Tests Method of Engineering Rock Masses (GB/T 50266-2013), indoor WD cycle tests were carried out on the rock samples by having the samples absorb natural water until saturation and then drying the samples. Each iteration of absorption, saturation and drying was recorded as a WD cycle.

Step 1 The samples were saturated with natural water as follows. The rock sample was placed into a water tank, after which water was added to 1/4 of the sample height; then, water was added to 1/2 and 3/4 of the sample height at 2 and 4 hours, respectively, and at 6 hours, water was added until the water level was 20 mm higher than the top surface of the sample. This process facilitated the escape of air trapped in the sample. Finally, the sample was allowed to absorb water freely for 48 hours.

Step 2 The samples were dried by being placed

into a drying oven and baked at a constant temperature of 105°C for 24 hours.

Step 3 The water-induced damage of rock in nature is the result of long-term action. To better simulate this process, the rock samples were subjected to 30 WD cycles, after which sample mass, longitudinal-wave velocity, uniaxial compressive strength, XRD and SEM tests were performed on the rock samples after 0, 5, 10, 15, 20, 25 and 30 WD cycles, and triaxial compression (4 and 8 MPa) tests were conducted on the rock samples after 0, 15 and 30 WD cycles to better explore the damage suffered by the rock samples. A flow chart of the testing methodology is depicted in Fig. 1.

3 Test Results of Damage after WD Cycles

An intelligent electronic scale with an accuracy of 0.01 g was used to weigh the rock samples after 0, 5, 10, 15, 20, 25 and 30 WD cycles. The variations in rock sample mass with the number of WD cycles are shown in Fig. 2. Fig. 2 (a) shows that the dry mass of the rock sample shows a two-stage decreasing trend with an increasing number of cycles; when the number of cycles reaches 30, the mass has decreased by 1.95%. In contrast, the saturated mass of the rock sample shows a two-stage increasing trend with an increasing number of cycles, and the mass increases by 6.98% at 30 cycles. The inflection point of their rate of change is the 15th WD cycle. The relationship between the rock sample mass and number of cycles can be fitted by a system of linear functions, and the following fitted equations can be obtained:

3.1 Changes in physical parameters

$$m_d^1 = -0.052n + 497.671 \quad n \leq 15, R^2 = 0.9659 \quad (1)$$

$$m_d^2 = -0.013n + 497.118 \quad 15 < n \leq 30, R^2 = 0.8606 \quad (2)$$

$$m_s^1 = 0.177n + 501.735 \quad n \leq 15, R^2 = 0.9818 \quad (3)$$

$$m_s^2 = 0.058n + 503.557 \quad 15 < n \leq 30, R^2 = 0.8881 \quad (4)$$

where m_d and m_s are the dry mass and saturated mass, respectively, after different numbers of WD cycles, n is the number of cycles, and R^2 is the coefficient of determination.

The saturated water content can be obtained by dividing the difference between the saturated mass and dry mass of a rock sample by the dry mass after different numbers of WD cycles. The variation with the number of WD cycles is shown in Fig. 2 (b), indicating that as the number of cycles rises, the saturated water contents of the rock samples show a two-stage increasing trend, with the inflection point of its rate of change appearing at 15 cycles and the saturated water content increasing by 111.52% at 30 cycles. The relationship between the saturated water content of the rock sample and the number of cycles can be fitted by a series of linear functions, and the following fitted equations can be obtained:

$$w^1 = 0.047n + 0.807 \quad n \leq 15, R^2 = 0.9861 \quad (5)$$

$$w^2 = 0.014n + 1.301 \quad 15 < n \leq 30, R^2 = 0.9029 \quad (6)$$

where w is the saturated moisture content after different numbers of WD cycles.

The longitudinal-wave velocity can be used as an index to reflect the compactness of a rock and both

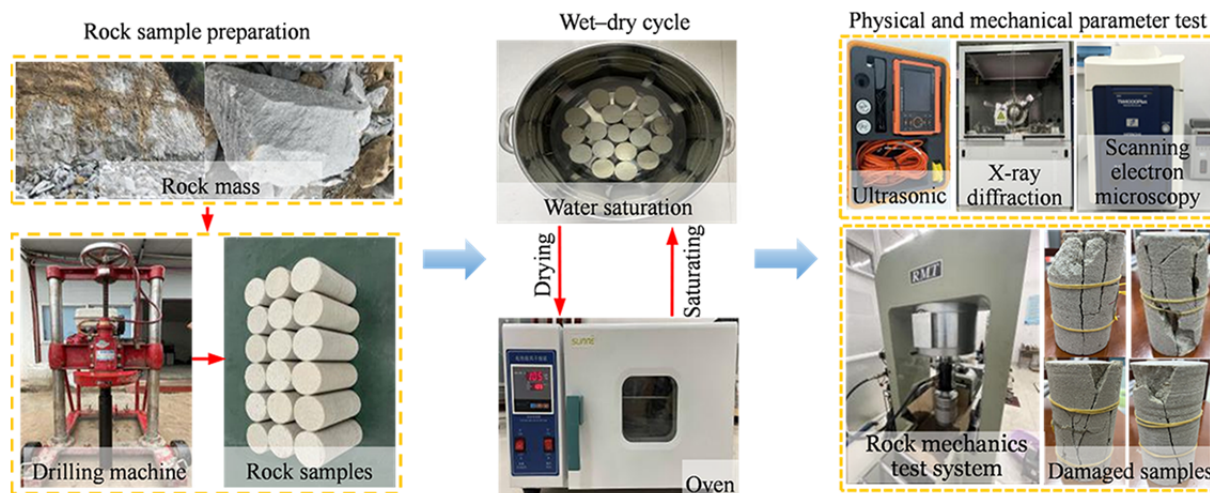


Fig. 1 Flow chart of rock sample preparation, wet-dry cycle test and physical and mechanical test.

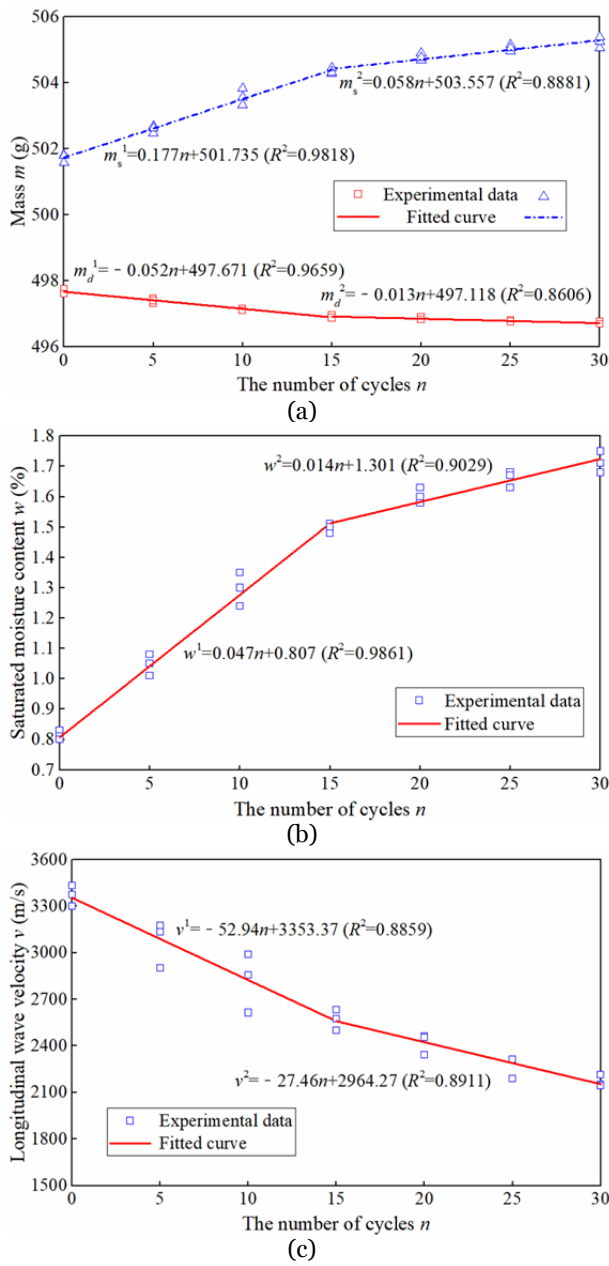


Fig. 2 Changes in physical parameters with the number of cycles: (a) mass, (b) saturated moisture content, (c) longitudinal-wave velocity.

the number and the size of pores (El-Gohary 2013). When the longitudinal-wave velocity is high, the rock sample is dense and contains relatively few pores; when the longitudinal-wave velocity is low, the rock sample is considered unconsolidated and porous. A nonmetallic acoustic detector was used to test the longitudinal-wave velocity of each rock sample after different numbers of WD cycles. The test results are shown in Fig. 2 (c), revealing that the longitudinal-wave velocities of the rock samples show a two-stage

decreasing trend, with the inflection point of its rate of change appearing at 15 cycles and the longitudinal-wave velocity decreasing by 35.62% at 30 cycles. These findings are evidence that irreversible damage occurs in rock samples under repeated WD cycles. The relationship between the longitudinal-wave velocity of the rock sample and the number of WD cycles can be fitted by a series of linear functions, and the following fitted equations can be obtained:

$$v^1 = -52.94n + 3353.37 \quad n \leq 15, R^2 = 0.8859 \quad (7)$$

$$v^2 = -27.46n + 2964.27 \quad 15 < n \leq 30, R^2 = 0.8911 \quad (8)$$

where v is the longitudinal-wave velocity after different numbers of WD cycles.

Ultimately, the relationships between the physical parameters of rock samples and the number of WD cycles can be fitted by linear functions, and the correlation coefficients are greater than 0.8606. The number of WD cycles has varying influences on different physical parameters, with its influence on the rock sample mass, longitudinal-wave velocity and saturated moisture content increasing in succession.

3.2 Changes in mechanical parameters

Uniaxial compression tests were carried out on the rock samples after 0, 5, 10, 15, 20, 25 and 30 WD cycles on an RMT-301 servo-hydraulic test machine, and the results are shown in Fig. 3. The data illustrate that increasing the number of cycles yields two-stage decreasing trends in the peak strength and elastic modulus of the rock samples and a two-stage increasing trend in the peak strain; the inflection point of the rate of change always appears at 15 cycles. At 30 cycles, the peak strength decreases by 24.28%, the elastic modulus decreases by 51.30% and the peak strain increases by 44.29%. Likewise, the relationships between the rock sample uniaxial test parameters and numbers of WD cycles can be fitted by various linear functions, and the following fitted equations can be obtained:

$$\sigma^1 = -1.092n + 80.018 \quad n \leq 15, R^2 = 0.9199 \quad (9)$$

$$\sigma^2 = -0.282n + 68.168 \quad 15 < n \leq 30, R^2 = 0.8541 \quad (10)$$

$$\varepsilon^1 = 0.121n + 7.256 \quad n \leq 15, R^2 = 0.9897 \quad (11)$$

$$\varepsilon^2 = 0.092n + 7.693 \quad 15 < n \leq 30, R^2 = 0.9972 \quad (12)$$

$$E^1 = -0.328n + 13.390 \quad n \leq 15, R^2 = 0.9833 \quad (13)$$

$$E^2 = -0.134n + 10.440 \quad 15 < n \leq 30, R^2 = 0.9615 \quad (14)$$

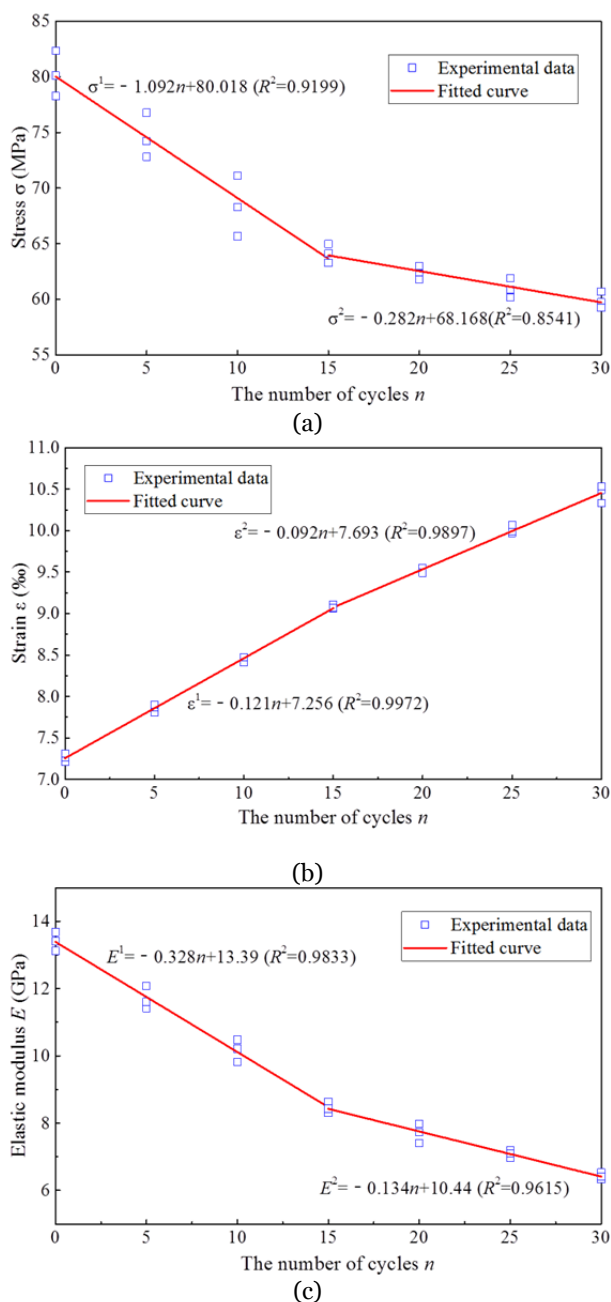


Fig. 3 Variations in uniaxial test parameters with the number of cycles: (a) peak intensity, (b) peak strain, (c) elastic modulus.

Next, according to the results of the uniaxial compression tests on the rock samples, the rock samples subjected to representative numbers of WD cycles (0, 15 and 30) were selected for triaxial tests, the results of which are shown in Table 1. The table suggest that under the same number of WD cycles, with increasing confining pressure, the peak strength, peak strain and elastic modulus of the rock samples gradually increase, while Poisson's ratio gradually

decreases. Moreover, under the same confining pressure, with an increase in the number WD cycles, the peak strength and elastic modulus of the rock samples gradually decrease, while the peak strain and Poisson's ratio gradually increase. Taking the confining pressure of 4 MPa as an example, the peak strength and elastic modulus of the rock samples in the first 15 WD cycles decrease by 32.48% and 33.98%, respectively, and the peak strain increases by 28.02%; after 15 WD cycles, the peak strength and elastic modulus of the rock samples decrease by 10.48% and 12.58%, respectively, and the peak strain increases by 23.50%. Thus, the influences of the number of WD cycles on the mechanical parameters of rock samples are similar to those on their physical parameters.

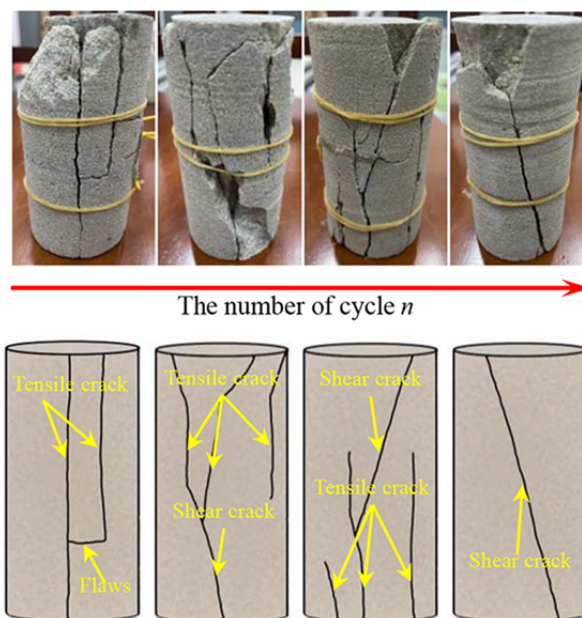


Fig. 4 Typical damage to a rock sample with an increasing number of wet-dry cycles.

Representative damaged rock samples were selected after different numbers of WD cycles for further analysis, as shown in Fig. 4. The failure mode of a rock sample changes with an increasing number of cycles. After a uniaxial compression test is performed on fresh rock, vertical tensile cracks appear on the surface of the rock sample, and the failure mode is tensile splitting failure. With an increasing number of WD cycles, the number of surface cracks on the rock samples increases obviously, manifesting mainly as vertical tensile cracks and shear cracks with different angles of inclination, and the failure mode is tensile-shear failure. After multiple WD cycles, shear cracks appear

on the surface of the rock sample, and the failure mode is shear failure. Thus, under the action of repeated WD cycles, the strength of the rock sample decreases, the deformation increases, and the failure mode changes from brittle tensile failure to plastic shear failure.

3.3 Microstructural evolution

A TM4000 plus scanning electron microscope was used to microscopically examine the rock samples after WD cycling. The test voltage was 15 kV, and the magnification was 2000, with the observations being carried out on the micron scale. The results are shown in Fig. 5, indicating that the surface of the original rock was flat; overall, the rock had few mineral particles, a dense structure, good integrity, and only a small number of initial microcracks and pores. After 5 WD cycles, the surface roughness of the rock sample increased, the cohesion of the structure was destroyed due to the development of microcracks, and the number of pores began to increase. After 10 WD cycles, transgranular cracks and pores propagated. At 15 WD cycles, the transgranular cracks widened, and a

throughgoing crack formed. At 20 WD cycles, the length, width and depth of the transgranular cracks further increased; in comparison, at 25 WD cycles, the cracks and pores in the rock samples gradually expanded and penetrated, and the surface shape became uneven. Finally, after 30 WD cycles, deep pores and cracks were observed in the rock samples, multiple throughgoing cracks were intertwined, and the structural integrity was seriously compromised. Therefore, the WD cycles caused serious irreversible damage to the rock.

3.4 Mineral and chemical composition changes

The changes in the macro- and microstructures of rock samples are of great significance and can be studied by evaluating the changes in their mineral compositions. Therefore, in this final analysis, the mineral compositions of the rock samples after different numbers of WD cycles were determined to reveal their damage. The mineral compositions of the rock samples were tested after 0, 5, 10, 15, 20, 25 and 30 WD cycles by a D8 Discovery X-ray diffractometer.

Table 1 Mechanical parameters at confining pressure of 4 and 8 MPa

| Confining pressure | Number of cycles <i>n</i> | Peak stress σ (MPa) | Peak strain ε (%) | Elastic modulus <i>E</i> (GPa) | Poisson's ratio μ | Internal friction angle β (°) |
|--------------------|---------------------------|----------------------------|-------------------------------|--------------------------------|-----------------------|-------------------------------------|
| 4 | 0 | 150.43 | 10.17 | 15.98 | 0.312 | 59.67 |
| | 15 | 101.56 | 13.02 | 10.49 | 0.332 | 57.67 |
| | 30 | 85.79 | 15.41 | 8.49 | 0.342 | 55.33 |
| 8 | 0 | 187.04 | 12.24 | 17.01 | 0.271 | 59.67 |
| | 15 | 152.48 | 15.50 | 12.75 | 0.291 | 57.67 |
| | 30 | 135.98 | 17.49 | 11.05 | 0.301 | 55.33 |

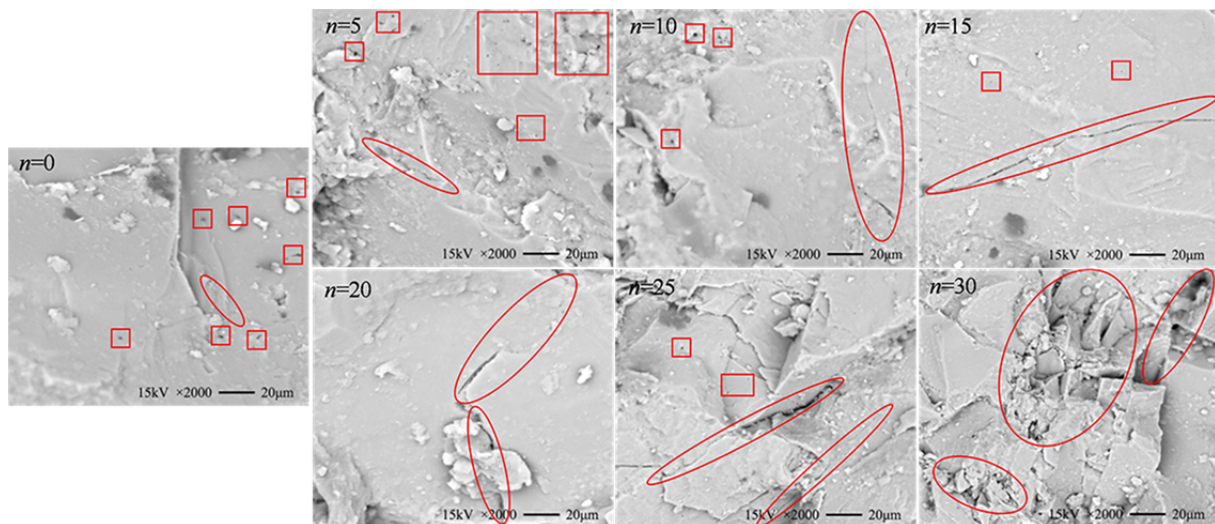
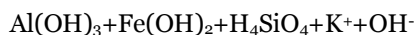
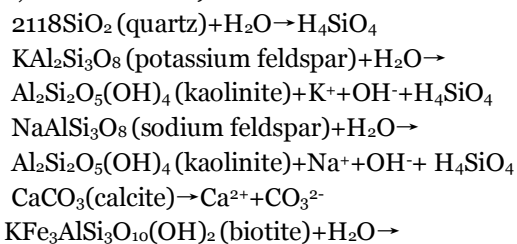


Fig. 5 SEM images of rock samples under different numbers of WD cycles.

The test results are shown in Table 2. Under natural conditions, the rock samples were composed mainly of feldspar, quartz, calcite, mica and clay minerals. After different numbers of WD cycles, the mineral compositions changed; in particular, the relative contents of feldspar, calcite and mica minerals decreased. After 30 WD cycles, the relative contents of feldspar, calcite, and mica minerals decreased by 4.5%, 3.2%, and 2.2%, respectively; in contrast, the relative contents of quartz and clay minerals increased by 5.8% and 4.1%, respectively, after 30 WD cycles.

Under the long-term action of WD cycling, different mineral components in rock samples undergo a series of chemical reactions with water, which is the fundamental reason for the changes in the relative contents of mineral components. This process is collectively known as hydrolysis (Feng et al. 2010; Wu et al. 2008):



Kaolinite produced by hydrolysis is characterized by its expansion upon absorbing water and its shrinkage upon losing water. Repeated WD cycles make kaolinite expand and contract frequently, promoting the development of cracks and pores in the rock. In addition, the chemical substances remaining after hydrolysis are easily soluble in water, resulting in the continuous removal of mineral components from the rock by water, which increases the hydrolysis contact surface and further aggravates the reaction. Thus, the cracks and pores connect and expand in the rock's microstructure, thereby degrading its macroscopic physical and mechanical properties.

In summary, WD cycles can affect the microstructure and mineral composition of rock, as depicted in Fig. 6. Before WD cycles, the mineral particles are inlaid and cemented together, and the particles are angular in shape; the structural plane is flat and smooth as a whole, with a small number of small pores and microcracks. After 1 to 15 WD cycles, the cementation between mineral particles is destroyed, forming erosion fractures, and small amounts of hydrolysis products are mixed in the fractures; microparticles appear on the structural plane, the roughness increases, and transgranular

Table 2 X-ray diffraction pattern and mineral analysis

| X-ray diffraction pattern | Relative mineral content (%) | | | | |
|---------------------------|------------------------------|--------|---------|------|---------------|
| | Feldspar | Quartz | Calcite | Mica | Clay minerals |
| | 10.7 | 66.5 | 8.5 | 2.1 | 12.2 |
| | 11.1 | 66.1 | 8.8 | 2.5 | 11.5 |
| | 11.7 | 65.7 | 9.1 | 2.8 | 10.7 |
| | 12.7 | 64.3 | 9.8 | 3.0 | 10.2 |
| | 14.1 | 62.0 | 11.1 | 3.7 | 9.1 |
| | 14.8 | 61.1 | 11.5 | 4.1 | 8.5 |
| | 15.2 | 60.7 | 11.7 | 4.3 | 8.1 |

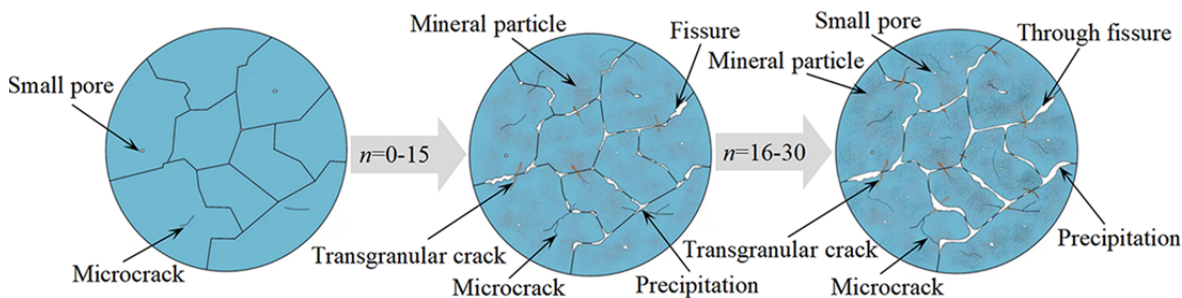


Fig. 6 Diagrams of the microstructural evolution after WD cycles.

cracks form between the mineral particles. After 16 to 30 WD cycles, the cementation components between mineral particles are further destroyed, the soluble substances generated by hydrolysis are extracted by water, forming erosion fractures throughout the structural plane, and the cracks and pores are obviously increased. In addition, the particles become increasingly rounded, which greatly reduces their cohesion and causes the rock to become unconsolidated and fragmented overall. Fig. 6 shows schematic diagrams reflecting the microstructural evolution of the test rock sample. The real situation may not be as serious, and more WD cycles may be required to achieve these graphical results, but this figure is nevertheless appropriate to describe the change trend of the microstructure of the rock sample after numerous WD cycles.

4 Constitutive Damage Model of Rock under WDL

4.1 WDL damage evolution equation

The damage of rock samples under repeated WD cycles is realized mainly through changes in macroparameters such as the longitudinal-wave velocity (Xu et al. 2020), elastic modulus (Du et al. 2019), porosity (Cui et al. 2021), and CT number (Liu et al. 2016).

The elastic modulus is easy to obtain experimentally and has obvious physical significance. Therefore, the change in the elastic modulus was adopted to define the WD cycle-induced damage D_n , and the following equation can be obtained:

$$D_n = 1 - \frac{E_n}{E_0} \tag{15}$$

where E_0 and E_n are the elastic moduli of rock before WD cycling and after n WD cycles, respectively.

The strength of rock microelements under WDL was assumed to follow a Weibull distribution, and three Weibull distribution function parameters were introduced (Gao and Xie 1996; Cao et al. 2013; Li et al. 2017). The following equation can be obtained:

$$F(x) = 1 - \exp\left[-\left(\frac{x-t}{\lambda}\right)^k\right] \quad (x \geq t) \tag{16}$$

where x is the strength of a rock microelement, t is the position parameter, k is the shape parameter, and λ is

the scale parameter.

Under different WD cycles, the rock Weibull parameters are as follows:

$$\begin{cases} t = t(n) \\ k = k(n) \\ \lambda = \lambda(n) \end{cases} \tag{17}$$

where $t(n)$, $k(n)$ and $\lambda(n)$ are the position parameter, shape parameter and proportion parameter of the Weibull distribution function after different numbers of WD cycles, respectively.

The development and propagation of microcracks and pores lead to the failure of rock microelements. With increasing microelement failure, the macroproperties of the rock deteriorate, and irreversible damage occurs. Therefore, the evolution of damage within rock parallels the failure evolution of microelements. The total rock damage D can thus be defined by the ratio of the number of failed rock microelements to the total number of microelements:

$$D = \frac{N_F}{N} \tag{18}$$

where N_F and N denote the number of failed microelements and the total number of microelements in the rock, respectively.

The strengths of rock microelements are randomly distributed. When the loading stress level is x , some microelements in the rock have been destroyed, the number of failures is N_F , and the following equation can be obtained:

$$N_F = N \int_0^x f(x) dx \tag{19}$$

where $f(x)$ is the probability density function of the Weibull distribution.

According to Eqs. (18) and (19), the following equation can be obtained:

$$D = \int_0^x f(x) dx \tag{20}$$

Substituting Eqs. (16) and (17) into Eq. (20), the total rock damage D can be obtained:

$$D = 1 - \exp\left[-\left(\frac{x-t(n)}{\lambda(n)}\right)^{k(n)}\right] \tag{21}$$

In Eq. (21), WD cycle-induced damage is considered in the total rock damage, which effectively reflects the damage evolution of rock under WDL.

4.2 WDL constitutive damage model

According to the Lemaitre strain equivalence principle (Lemaitre 1985) and effective stress principle, the relationship between the nominal stress in the triaxial compression test σ_i and the effective stress σ_i^* can be obtained as follows:

$$\sigma_i = \sigma_i^* (1 - D) \quad (i=1,2,3) \quad (22)$$

The results of the triaxial tests show that the strength of rock is not completely lost after failure, as it still has a certain bearing capacity, which is called its residual strength. However, residual strength is not considered in Eq. (22). When a rock is completely destroyed, the total damage D is 1, and the nominal stress in Eq. (22) is 0, which is inconsistent with the actual test results. Therefore, it is necessary to introduce a correction factor ω ($0 < \omega < 1$) to modify Eq. (22) (Cao et al. 2013; Xu et al. 2018). The corrected relationship between nominal stress σ_i and effective stress σ_i^* can be obtained as follows:

$$\sigma_i = \sigma_i^* (1 - \omega D) \quad (23)$$

When a rock is completely destroyed and the total damage D is 1, the nominal stress in Eq. (23) is not 0; thus, this equation better reflects the residual strength as a mechanical index.

The root cause of rock failure is microelement failure. Therefore, it is important to select the rock microelement failure criterion. The D–P yield criterion is simple and practical with few material parameters (Cao et al. 1998; Xu et al. 2002; Li et al. 2007). Therefore, the D–P yield criterion was used as the microelement failure criterion in this paper, and the following equation can be obtained:

$$x = \alpha I_1^* + \sqrt{J_2^*} \quad (24)$$

where $\alpha = \sin\beta / (9 + 3\sin^2\beta)^{0.5}$ and β is the internal friction angle. I_1^* is the first invariant of the stress tensor, $I_1^* = \sigma_1^* + \sigma_2^* + \sigma_3^*$. J_2^* is the second invariant of the effective stress deviation, $J_2^* = ((\sigma_1^* - \sigma_2^*)^2 + (\sigma_2^* - \sigma_3^*)^2 + (\sigma_1^* - \sigma_3^*)^2) / 6$.

The generalized form of Hooke's law is as follows:

$$\varepsilon_i = \frac{1}{E} \left[\sigma_i^* - \mu (\sigma_j^* + \sigma_k^*) \right] \quad (i, j, k=1,2,3) \quad (25)$$

where ε_i , μ and E are the strain, Poisson's ratio and elastic modulus, respectively.

According to Eqs. (23), (24) and (25), the following can be obtained:

$$\begin{aligned} x &= \alpha I_1^* + \sqrt{J_2^*} \\ &= \frac{(\sigma_1 - \sigma_3) E \varepsilon_1 \sin \beta}{(\sigma_1 - \mu(\sigma_2 + \sigma_3)) \sqrt{9 + 3 \sin^2 \beta}} \\ &\quad + \frac{E \varepsilon_1 (\sigma_1 - \sigma_3)}{\sqrt{3} (\sigma_1 - \mu(\sigma_2 + \sigma_3))} \end{aligned} \quad (26)$$

According to Eqs. (21)–(26), the rock constitutive damage equation considering the action of WD cycles can be obtained:

$$\begin{aligned} \sigma_i &= E_0 (1 - D_n) \varepsilon_i \\ &\times \left\{ 1 - \omega + \omega \exp \left[- \left(\frac{\alpha I_1^* + \sqrt{J_2^*} - t(n)}{\lambda(n)} \right)^{k(n)} \right] \right\} \\ &+ \mu (\sigma_j + \sigma_k) \end{aligned} \quad (27)$$

The essence of rock deformation and failure is the development, propagation and penetration of microcracks and pores. When the stress level is less than the initial stress, no cracks or pores develop in the rock, and the rock damage value is 0. Therefore, there is a stress threshold in the evolution of rock damage, and the rock is damaged only when the stress level is higher than this threshold.

A previous study (Cai et al. 2004) postulated that the typical stress–strain curve of rock can be divided into five stages: a crack closure stage, an elastic stage, a stable crack growth stage, a crack coalescence stage, and a postpeak stage. The point separating the linear elastic stage from the stable crack growth stage is the crack generation point, and the corresponding stress and strain are the crack initiation stress σ_{ci} and crack initiation strain ε_{ci} , respectively. The damage evolution equation governing the whole process of rock deformation and failure can be expressed as follows:

$$D = \begin{cases} 0 & (\sigma < \sigma_{ci}) \\ 1 - \exp \left[- \left(\frac{\alpha I_1^* + \sqrt{J_2^*} - t(n)}{\lambda(n)} \right)^{k(n)} \right] & (\sigma \geq \sigma_{ci}) \end{cases} \quad (28)$$

When the rock stress level is higher than the stress threshold, the WDL constitutive damage model is given by Eq. (27). When the rock stress level is lower than the stress threshold, this quadratic function can be used to fit the data according to the stages of the typical stress–strain curve of a rock, and the following equation can be obtained:

$$\sigma_i = a\varepsilon_i^2 + b\varepsilon_i \quad (\varepsilon < \varepsilon_{ci}) \quad (29)$$

The comprehensive WDL constitutive damage model pertaining to the whole process of rock deformation and failure can be obtained by Eqs. (27) and (29) and can be expressed as follows:

$$\sigma_i = \begin{cases} a\varepsilon_i^2 + b\varepsilon_i & (\varepsilon < \varepsilon_{ci}) \\ E_0(1-D_n)\varepsilon_i & \\ \times \left\{ 1 - \omega + \omega \exp \left[- \left(\frac{\alpha I_1^* + \sqrt{J_2^*} - t(n)}{\lambda(n)} \right)^{k(n)} \right] \right\} & \\ + \mu(\sigma_j + \sigma_k) & (\varepsilon \geq \varepsilon_{ci}) \end{cases} \quad (30)$$

4.3 Constitutive model parameters

The WDL constitutive damage model of rock contains some unknown parameters that need to be determined in combination with the uniaxial and triaxial test data of the rock, and the continuity of the piecewise function should be considered. For simplicity and convenience, Eq. (30) can be written as:

$$\sigma_i = \begin{cases} a\varepsilon_i^2 + b\varepsilon_i & (\varepsilon < \varepsilon_{ci}) \\ E\varepsilon_i & \\ \times \left\{ 1 - \omega + \omega \exp \left[- \left(\frac{\alpha I_1^* + \sqrt{J_2^*} - t}{\lambda} \right)^k \right] \right\} & \\ + \mu(\sigma_j + \sigma_k) & (\varepsilon \geq \varepsilon_{ci}) \end{cases} \quad (31)$$

4.3.1 Weibull distribution parameters t , k , and λ

The position parameter t represents the starting point of rock damage development, that is, the crack initiation stress point (σ_{ci} , ε_{ci}). At this time, the rock damage is 0. Considering that the test involves conventional triaxial compression, $\sigma_2 = \sigma_3$. According to Eq. (17) and Eq. (28):

$$t = \lim_{\sigma \rightarrow \sigma_{ci}} \alpha I_1^* + \sqrt{J_2^*} = \frac{(\sigma_{ci} - \sigma_3) E \varepsilon_{ci} \sin \beta}{(\sigma_{ci} - 2\mu\sigma_3) \sqrt{9 + 3 \sin^2 \beta}} + \frac{E \varepsilon_{ci} (\sigma_{ci} - \sigma_3)}{\sqrt{3} (\sigma_{ci} - 2\mu\sigma_3)} \quad (32)$$

The shape parameter k and proportion parameter λ can be obtained according to two geometric conditions at the peak stress-strain point (σ_c , ε_c), that is, ① $\varepsilon = \varepsilon_c, \sigma = \sigma_c$ and ② $\varepsilon = \varepsilon_c, d\sigma_c/d\varepsilon_c = 0$.

According to geometric condition ①, the following equation can be obtained:

$$\sigma_c = E\varepsilon_c \left\{ 1 - \omega + \omega \exp \left[- \left(\frac{\alpha I_1^* + \sqrt{J_2^*} - t}{\lambda} \right)^k \right] \right\} + 2\mu\sigma_3 \quad (33)$$

According to geometric condition ②, the following equation can be obtained:

$$\frac{d\sigma_c}{d\varepsilon_c} = E \left\{ 1 - \omega + \omega \exp \left[- (M/\lambda)^k \right] \right\} - kE\varepsilon_c \omega (N/\lambda) (M/\lambda)^{k-1} \exp(-M^k) = 0 \quad (34)$$

where

$$M = \frac{(\sigma_c - \sigma_3) E \varepsilon_c \sin \beta}{(\sigma_c - 2\mu\sigma_3) \sqrt{9 + 3 \sin^2 \beta}} + \frac{E \varepsilon_c (\sigma_1 - \sigma_3)}{\sqrt{3} (\sigma_c - 2\mu\sigma_3)} - t$$

and $N = \frac{(\sigma_c - \sigma_3) E \sin \beta}{(\sigma_c - 2\mu\sigma_3) \sqrt{9 + 3 \sin^2 \beta}} + \frac{E (\sigma_c - \sigma_3)}{\sqrt{3} (\sigma_c - 2\mu\sigma_3)}$.

Applying Eqs. (26), (31) and (34) simultaneously, the following equation can be obtained:

$$\begin{cases} k = \frac{M(\sigma_c - 2\mu\sigma_3)}{N\varepsilon_c [\sigma_c - 2\mu\sigma_3 + E\varepsilon_c(\omega - 1)] \ln \frac{\omega E \varepsilon_c}{\sigma_c - 2\mu\sigma_3 + E\varepsilon_c(\omega - 1)}} \\ \lambda = \left(\frac{(M)^k}{\ln \frac{\omega E \varepsilon_c}{\sigma_c - 2\mu\sigma_3 + E\varepsilon_c(\omega - 1)}} \right)^{\frac{1}{k}} \end{cases} \quad (35)$$

4.3.2 Quadratic function parameters a and b

When the rock stress does not reach the damage threshold, the stress-strain curve can be fitted by a quadratic function. According to the continuity of the piecewise function and Eq. (31), the following equation can be obtained:

$$a\varepsilon_{ci}^2 + b\varepsilon_{ci} = E\varepsilon_{ci} \times \left\{ 1 - \omega + \omega \exp \left[- \left(\frac{Y}{\lambda} \right)^k \right] \right\} + 2\mu\sigma_3 \quad (36)$$

$$Y = \frac{(\sigma_{ci} - \sigma_3) E \varepsilon_{ci} \sin \beta}{(\sigma_{ci} - 2\mu\sigma_3) \sqrt{9 + 3 \sin^2 \beta}} + \frac{E \varepsilon_{ci} (\sigma_{ci} - \sigma_3)}{\sqrt{3} (\sigma_{ci} - 2\mu\sigma_3)} - t$$

Considering that the rock is a concave function in the crack closure stage, by letting the quadratic function pass through the fixed point (0.5 ε_{ci} , 0.5 σ_{ci}), the following equation can be obtained:

$$a\varepsilon_{ci}^2 + 2b\varepsilon_{ci} = 2\sigma_{ci} \quad (37)$$

The values of a and b can be obtained by solving Eqs. (36) and (37) simultaneously.

4.3.3 Damage threshold

After a certain number of WD cycles, a rock

contains some initial cracks and pores. At the initial stage of loading, these cracks and pores are gradually closed. After entering the linear elastic stage, the rock undergoes elastic deformation but not plastic deformation. When the load strength reaches the maximum value of the linear elastic stage, the rock begins to produce new cracks. The point on the stress–strain curve corresponding to this value is the damage threshold, the corresponding stress is the initiation stress, and the strain is the initiation strain. In an actual test, however, it is difficult to obtain an accurate damage threshold. Many scholars have conducted relevant research (Tuncay et al. 2008; Brace et al. 1966; Holcomb et al. 1987; Martin et al. 1993), and it is widely believed that the crack initiation stress is approximately 30% ~ 50% of the peak stress. Based on this research, 40% of the peak stress was taken as the crack initiation stress in this paper.

5 Verification of the Constitutive Damage Model

According to the uniaxial and triaxial test data and the constitutive model parameters described in Section 4.3, the values of the constitutive model parameters under different conditions are obtained, and the results are shown in Table 3. After substituting the data in Table 3 into the WDL constitutive damage model, the obtained theoretical curve is compared with the test curve, as shown in Fig. 7.

Table 3 Values of the wet–dry loading (WDL) constitutive model parameters

| n | σ_3 (MPa) | t | k | λ | a | b | w |
|-----|------------------|--------|-------|-----------|-------|-------|-------|
| 0 | | 28.523 | 4.670 | 74.904 | 2.608 | 6.752 | 1.000 |
| 15 | 0 | 25.998 | 4.497 | 56.657 | 1.341 | 2.516 | 1.000 |
| 30 | | 21.448 | 6.908 | 47.580 | 0.585 | 4.201 | 1.000 |
| 0 | 4 | 54.432 | 9.335 | 102.471 | 1.772 | 9.682 | 0.665 |
| 15 | 4 | 45.868 | 2.893 | 94.608 | 1.677 | 2.724 | 0.800 |
| 30 | | 34.645 | 3.820 | 80.224 | 1.007 | 3.605 | 0.800 |
| 0 | 8 | 68.416 | 7.101 | 138.911 | 1.808 | 9.688 | 0.750 |
| 15 | 8 | 55.376 | 4.229 | 138.240 | 0.823 | 9.335 | 0.800 |
| 30 | | 57.510 | 2.805 | 136.140 | 1.934 | 0.490 | 0.850 |

Fig. 7 shows that the theoretical curve is in good agreement with the test data. The WDL constitutive damage model established in this paper can reflect the stress–strain relationship in the process of rock deformation and failure. On the whole, the error between the theoretical curve and the test data is within the allowable range of practical applications, so

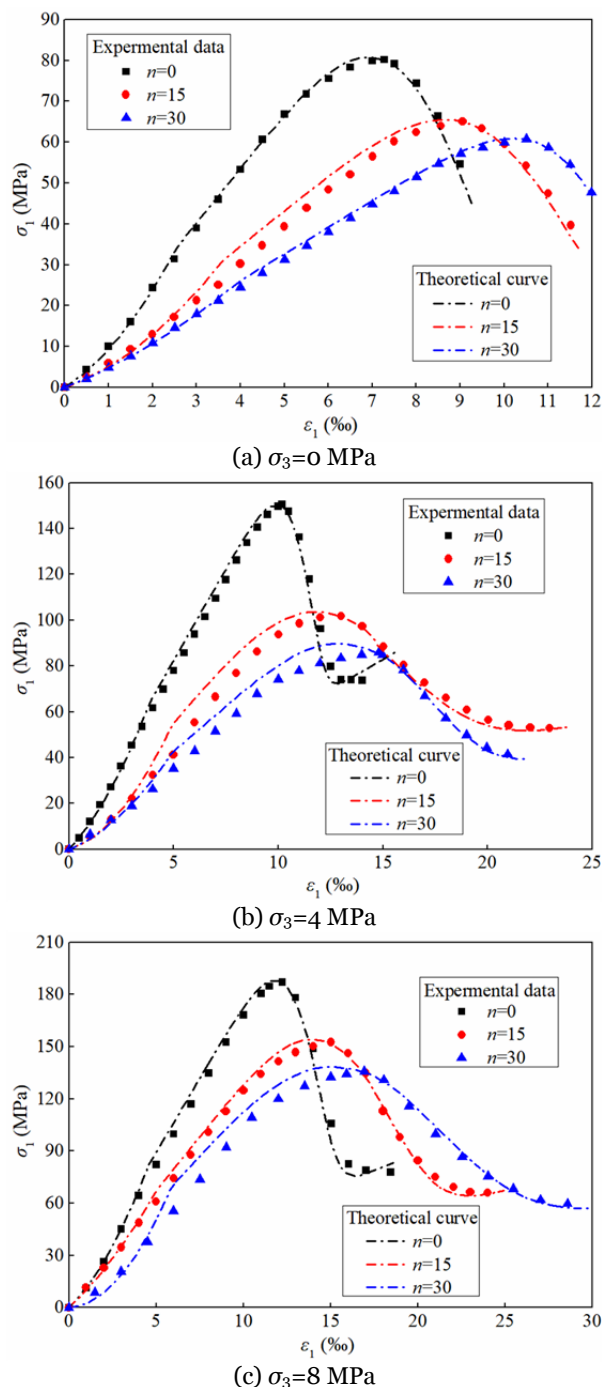


Fig. 7 Comparison between the theoretical curve (WDL constitutive damage model) and test data (Laboratory test).

the proposed model can provide reference value for an actual project to a certain extent.

The correction coefficient w is an empirical parameter that was fitted according to the test data. Taking $n=15$ and $\sigma_3=8$ MPa as an example, the rock stress–strain curves corresponding to different

correction coefficients w are shown in Fig. 8, illustrating that w has an important influence on the rock stress–strain curve. The smaller the correction coefficient w is, the slower the decline in the postpeak stage of the corresponding stress–strain curve and the greater the residual strength. However, w has little effect on the stress–strain curve before the peak stress.

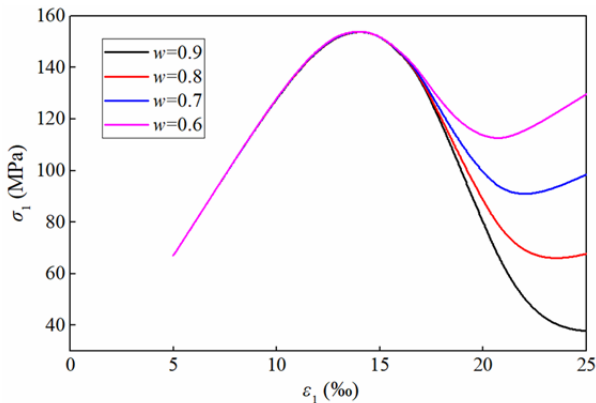


Fig. 8 Stress–strain curves corresponding to different correction coefficients w .

6 Conclusions and Suggestions

(1) Macroscopically, with an increase in the number of WD cycles, the dry mass, longitudinal-wave velocity, peak strength and elastic modulus of rock samples gradually decrease, whereas the saturated mass, saturated moisture content and peak strain of rock samples gradually increase; moreover, the rate of change presents two stages, the inflection point of their rate of change is the 15th WD cycle. The influences of the number of WD cycles on the physical and mechanical parameters increase in the order of saturated moisture content > elastic modulus > peak strain > longitudinal-wave velocity > peak strength > saturated mass > dry mass. The two stages are fitted by linear functions, the fitting coefficient $R^2 \geq 0.8541$, and the failure mode changes from brittle tension failure to plastic shear failure.

(2) Microscopically, with an increase in the number WD cycles, the rock sample structure tends to

become increasingly unconsolidated, the surface morphology changes from flat to rough, and the structural integrity worsens. After 15 cycles, microcracks develop into throughgoing cracks, and after 30 cycles, multiple throughgoing cracks are intertwined, resulting in serious and irreversible damage to the rock sample. Moreover, hydrolysis changes the relative contents of minerals in rock samples, which is the fundamental reason for the microstructural changes. Microscopic changes in rock samples ultimately lead to macroscopic changes in their physical and mechanical parameters.

(3) In terms of the constitutive damage model, first, by introducing a WD cycle-induced damage variable and assuming that the strengths of rock microelements obey a Weibull distribution, an equation reflecting the total WDL damage evolution in a rock is established. Then, according to the Lemaitre strain equivalence principle and the concept of effective stress, by introducing a residual strength correction coefficient and taking the D–P yield criterion as the basis for the failure of rock microelements, the rock WDL constitutive damage model is established, and a method for determining the model parameters is proposed. Finally, the theoretical curve is compared with the experimental data, demonstrating good agreement. Thus, the proposed model can reflect the stress–strain relationship in the evolution of rock deformation and failure.

Note that the theoretical curve obtained from the rock WDL constitutive damage model established in this paper has nonderivable points; that is, the theoretical curve is not smooth at the damage threshold point. In addition, completely homogeneous sandstone was selected as the research object in this paper, whereas sandstones featuring bedding and joints are often encountered in practical engineering, which can lead to changes in the applicability and accuracy of the constitutive model. Therefore, it is necessary to perform an in-depth analysis and discussion of the above contents in follow-up research.

Acknowledgements

This work was supported by the National Natural Science Foundation of China (Grant No. 52108367) and Guangxi University Young and middle-aged

teachers' basic scientific research ability improvement project (2020ky01011).

References

- An WB, Wang LG, Chen H (2020) Mechanical properties of weathered feldspar sandstone after experiencing dry-wet cycles. *Adv Mater Sci Eng* 2020.
<https://doi.org/10.1155/2020/6268945>
- Brace WF, Jr B, Scholz C (1966) Dilatancy in the fracture of crystalline rocks. *J Geophys Resour* 71(16): 39-53.
<https://doi.org/10.1029/JZ071i016p03939>
- Cao WG, Fang ZL, Tang XJ (1998) A study of statistical constitutive model for soft and damage rocks. *Chin J Rock Mech Eng* 17(6): 628-633. (In Chinese)
- Cao RL, He SH, Wei J, et al. (2013) Study of modified statistical damage softening constitutive model for rock considering residual strength. *Rock Soil Mech* 34(6): 1652-1660. (In Chinese)
<https://doi.org/10.16285/j.rsm.2013.06.018>
- Cai M, Kaiser PK, Tasaka Y, et al. (2004) Generalized crack initiation and crack damage stress thresholds of brittle rock masses near underground excavations. *Int J Rock Mech Min* 41(5): 833-847.
<https://doi.org/10.1016/j.ijrmms.2004.02.001>
- Chen WW, Liao RX, Wang N, et al. (2019) Effects of experimental frost-thaw cycles on sandstones with different weathering degrees: a case from the Bingling Temple Grottoes, China. *B Eng Geol Environ* 78(7): 5311-5326.
<https://doi.org/10.1007/s10064-018-01454-2>
- Chen XX, He P, Qin Z (2018) Damage to the microstructure and strength of altered granite under wet-dry cycles. *Symmetry-Basel* 10(12): 716.
<https://doi.org/10.3390/sym10120716>
- Cui K, Gu X, Wu GP, et al. (2021) Study on the characteristics and mechanism of dry-wet damage of rock carrier in Helan mouths rock paintings under different conditions. *Chin J Rock Mech Eng* 40(06): 1236-1247. (In Chinese)
<https://doi.org/10.13722/j.cnki.jrme.2020.1096>
- Du B, Bai HB (2019) A damage constitutive model of red sandstone under coupling of wet-dry cycles and impact load. *Shock Vib* 2019.
<https://doi.org/10.1155/2019/7692424>
- El-Gohary MA (2013) Evaluation of treated and un-treated Nubia sandstone using ultrasonic as a non-destructive technique. *J Archaeol Sci* 40(4): 2190-2195.
<https://doi.org/10.1016/j.jas.2012.12.023>
- Fang JC, Deng HF, Qi Y, et al. (2019) Analysis of changes in the micromorphology of sandstone joint surface under dry-wet cycling. *Adv Mater Sci Eng* 2019.
<https://doi.org/10.1155/2019/8758203>
- Fener M (2011) The effect of rock sample dimension on the P-wave velocity. *J Nondestruct Eval* 30(2): 99-105.
<https://doi.org/10.1007/s10921-011-0095-7>
- Feng XT, Ding WX, Cui Q, et al. (2010) Coupled chemical-stress effect on rock fracturing process. Beijing: Beijing Science Press. pp 10-15. (In Chinese)
- Gao F, Xie HP (1996) Statistically fractal strength theory for brittle materials. *Acta Mech Solida Sin* 9(1): 42-51.
[https://doi.org/10.1016/1359-6454\(95\)00246-4](https://doi.org/10.1016/1359-6454(95)00246-4)
- GB/T 50266-2013 (2013) Standard for Test Method of Engineering Rock Mass. (In Chinese)
- Gholamreza K, Yasin A (2015) Influence of wet-dry, freeze-thaw, and heat-cool cycles on the physical and mechanical properties of Upper Red sandstones in central Iran. *B Eng Geol Environ* 74(4): 1287-1300.
<https://doi.org/10.1007/s10064-014-0691-8>
- Holcomb DJ, Costin LS (1987) Damage in brittle materials: experimental methods. In: Lamb JP (ed.), *Proceedings of the 10th U.S. National Congress of Applied Mechanics*.
- Hu M, Liu YX, Song LB, et al. (2018) Constitutive model and damage evolution of mudstone under the action of dry-wet cycles. *Adv Civ Eng* 2018.
<https://doi.org/10.1155/2018/9787429>
- Lee CH, Jo YH, Kim J (2011) Damage evaluation and conservation treatment of the tenth century Korean rock-carved Buddha statues. *Environ Earth Sci* 64(1):1-14.
<https://doi.org/10.1007/s12665-010-0809-7>
- Lemaitre J (1984) How to use damage mechanics. *Nucl Eng Des* 80(3): 233-245.
[https://doi.org/10.1016/0029-5493\(84\)90169-9](https://doi.org/10.1016/0029-5493(84)90169-9)
- Li SC, Xu J, Li KG, et al. (2007) Study on damages constitutive model of rocks based on Weibull distribution. *J Hunan Univ Sci Technol (Nat Sci Ed)* 22(4): 65-68. (In Chinese)
- Li TB, Gao MB, Chen GQ, et al. (2017) A thermal-mechanical-damage constitutive model for hard brittle rocks and its preliminary application. *Chin J Geotech Eng* 39(8): 1477-1484. (In Chinese)
- Li X, Cao WG, Su YH (2012) A Statistical damage constitutive model for softening behavior of rocks. *Eng Geol* 143: 1-17.
<https://doi.org/10.1016/j.enggeo.2012.05.005>
- Liu XR, Jin MH, Li DL, et al. (2018) Strength deterioration of a shaly sandstone under dry-wet cycles: a case study from the Three Gorges Reservoir in China. *B Eng Geol Environ* 77(4): 1607-1621.
<https://doi.org/10.1007/s10064-017-1107-3>
- Liu XR, Wang ZJ, Fu Y, et al. (2016) Macro/Microtesting and damage and degradation of sandstones under dry-wet cycles. *Adv Mater Sci Eng* 2016.
<https://doi.org/10.1155/2016/7013032>
- Martin CD (1993) The strength of massive Lac du Bonnet granite around underground opening. PhD thesis, University of Manitoba.
- Mckenzie CK, Stacey GP, Gladwin MT (1982) Ultrasonic characteristics of a rock mass. *Int J Rock Mech Min* 19(1): 25-30.
[https://doi.org/10.1016/0148-9062\(82\)90707-0](https://doi.org/10.1016/0148-9062(82)90707-0)
- Meng YY, Jing HW, Yin Q, et al. (2020) Investigation on mechanical and AE characteristics of yellow sandstone undergoing wetting-drying cycles. *KSCE J Civ Eng* 24(11): 3267-3278.
<https://doi.org/10.1007/s12205-020-0572-6>
- Ni HB, Zhang LP, Zhang DR, et al. (2008) Weathering of pisha-sandstones in the wind-water erosion crisscross region on the Loess Plateau. *J Mt Sci* 5(4): 340-349.
<https://doi.org/10.1007/s11629-008-0218-5>
- Qin Z, Chen XX, Fu HL (2018) Damage features of altered rock subjected to drying-wetting cycles. *Adv Civ Eng* 2018.
<https://doi.org/10.1155/2018/5170832>
- Özbek A (2013) Investigation of the effects of wetting-drying and freezing-thawing cycles on some physical and mechanical properties of selected ignimbrites. *B Eng Geol Environ* 73(2): 595-609.
<https://doi.org/10.1007/s10064-013-0519-y>
- Shen PW, Tang HM, Ning YB, et al. (2019) A damage mechanics based on the constitutive model for strain-softening rocks. *Nucl Eng Des* 80(3): 233-245.
<https://doi.org/10.1016/j.engfracmech.2019.106521>
- Shen ZL, Wang YX (2002) Review and outlook of water-rock interaction studies. *Ear Sci* 27(2):127-133. (In Chinese)
- Shen ZL, Zhong ZS, Wen DG, et al. (1993) Advances in geochemical thermodynamics and kinetics of water-rock interaction since the 1980s. *Proceedings of the First China Conference on Thermodynamics of Natural Action*. Beijing. (In Chinese)
- Trenhaile AS (2014) Modelling tidal notch formation by wetting and drying and salt weathering. *Geomorphology* 224: 139-151.
<https://doi.org/10.1016/j.geomorph.2014.07.014>
- Tuncay E, Ulusay R (2008) Relation between Kaiser effect levels

- and pre-stresses applied in the laboratory. *Int J Rock Mech Min* 45(3): 524-537.
<https://doi.org/10.1016/j.ijrmms.2007.07.013>
- Vilhelm J, Rudajev V, Lokajiček T, et al. (2013) Velocity dispersion in fractured rocks in a wide frequency range. *J Appl Geophys* 90:138-146.
<https://doi.org/10.1016/j.jappgeo.2013.01.010>
- Wang LQ, Yin YP, Huang BL, et al. (2020) A study of the treatment of a dangerous thick submerged rock mass in the three gorges reservoir area. *B Eng Geol Environ* 79: 2579-2590.
<https://doi.org/10.1007/s10064-020-01724-y>
- Wang LQ, Yin YP, Huang BL, et al. (2020) Damage evolution and stability analysis of the Jianchuandong Dangerous Rock Mass in the Three Gorges Reservoir Area. *Eng Geol* 265.
<https://doi.org/10.1016/j.enggeo.2019.105439>
- Wang XS, Wan L, Huang JZ, et al. (2014) Variable temperature and moisture conditions in Yungang Grottoes, China, and their impacts on ancient sculptures. *Environ Earth Sci* 72(8): 3079-3088.
<https://doi.org/10.1007/s12665-014-3213-x>
- Wang ZL, Li YC, Wang JG (2007) A damage-softening statistical constitutive model considering rock residual strength. *Comput Geosci-UK* 33(1): 1-9.
<https://doi.org/10.1016/j.cageo.2006.02.011>
- Wang ZJ, Liu XR, Yang X, et al. (2017) An improved Duncan-Chang constitutive model for sandstone subjected to drying-wetting cycles and secondary development of the model in FLAC^{3D}. *Arab J Sci Eng* 42(3): 1265-1282.
<https://doi.org/10.1007/s13369-016-2402-1>
- Weibull W (1951) A statistical distribution function of wide applicability. *ASME Journal of Applied Mechanics* 18:293-297.
- Wu XY, Zhu BL, Luo J (2008) Weathering process of black rock stratum and its thermodynamic analysis. Beijing: Science Press 15-54. (In Chinese)
- Xie KN, Jiang DY, Sun ZG, et al. (2018) NMR, MRI and AE statistical study of damage due to a low number of wetting-drying cycles in sandstone from the Three Gorges Reservoir Area. *Rock Mech and Rock Eng* 51: 3625-3634.
<https://doi.org/10.1007/s00603-018-1562-6>
- Xu WY, Wei LD (2002) Study on statistical damage constitutive model of rock. *Chin J Rock Mech Eng* 21(6): 787-791. (In Chinese)
- Xu XL, Karakus M, Gao F, et al. (2018) Thermal damage constitutive model for rock considering damage threshold and residual strength. *J Cent South Univ* 25(10): 2523-2536.
<https://doi.org/10.1007/s11771-018-3933-2>
- Xu ZH, Feng GL, Sun QC, et al. (2020) A modified model for predicting the strength of drying-wetting cycled sandstone based on the p-wave velocity. *Sustainability-Basel* 12(14):340-349.
<https://doi.org/10.3390/su12145655>
- Yuan W, Liu XR, Fu Y (2018) Study on deterioration of strength parameters of sandstone under the action of dry-wet cycles in acid and alkaline environment. *Arab J Sci Eng* 43(1): 335-348.
<https://doi.org/10.1007/s13369-017-2870-y>
- Zeng ZX, Kong LW (2019) Effect of wetting-drying-freezing-thawing cycles on the swelling behaviour of the Yanji mudstone. *Environ Earth Sci* 78(15).
<https://doi.org/10.1007/s12665-019-8447-1>
- Zhang JK, Li Z, Li L, et al. (2021) Study on weathering mechanism of sandstone statues in Southwest China: example from the sandstone of Niche of Sakyamuni Entering Nirvana at Dazu Rock Carvings. *Nat Hazards* 108(1): 775-797.
<https://doi.org/10.1007/s11069-021-04705-w>
- Zhang ZH, Jiang QH, Zhou CB, et al. (2014) Strength and failure characteristics of Jurassic Red-Bed sandstone under cyclic wetting-drying conditions. *Geophys J Int* 198(2): 1034-1044.
<https://doi.org/10.1093/gji/ggu181>
- Zhao YF, Ren S, Jiang DY, et al. (2018) Influence of wetting-drying cycles on the pore structure and mechanical properties of mudstone from Simian Mountain. *Constr Build Mater* 191: 923-931.
<https://doi.org/10.1016/j.conbuildmat.2018.10.069>